/
Article / Book Information

Title	Experimental Evaluation of Intersymbol Interference in Non-Far Region Transmission using a Large Array Antenna in the Millimeter-Wave Band
Authors	Tuchjuta Ruckkwaen, Takashi Tomura, Kiyomichi Araki, Jiro Hirokawa, Makoto Ando
Citation	IEICE Transactions on Communications, Vol. E103-B, No. 10, pp. 1136-1146
Pub. date	2020, 10
Copyright	Copyright (c) 2020 Institute of Electronics, Information and Communication Engineers.

PAPER

Experimental Evaluation of Intersymbol Interference in Non-Far Region Transmission using a Large Array Antenna in the Millimeter-Wave Band

Tuchjuta RUCKKWAEN[†a)], *Student Member*, Takashi TOMURA[†], *Member*, Kiyomichi ARAKI[†], Jiro HIROKAWA[†], *and* Makoto ANDO[†], *Fellows*

SUMMARY Intersymbol interference (ISI) is a significant source of degradation in many digital communication systems including our proposed non-far region communication system using large array antennas in the millimeter-wave band in which the main cause of ISI can be attributed to the path delay differences among the elements of an array antenna. This paper proposes a quantitative method to evaluate the ISI estimated from the measured near-field distribution of the array antenna. The influence of the uniformity in the aperture field distribution in ISI is discussed and compared with an ideally uniform excitation. The reliability of the proposed method is verified through a comparison with another method based on direct measurements of the transmission between the actual antennas. Finally, the signal to noise plus interference is evaluated based on the estimated ISI results and ISI is shown to be the dominant cause of the degradation in the reception zone of the system.
key words: intersymbol interference (ISI), non-far region, large array antenna, signal to noise plus interference (SINR)

1. Introduction

Given the boom in internet services, the demand for high-speed wireless communication is increasing. This has led to the development of several new wireless communication technologies that offer higher data transmission rates. The compact range communication proposed in [1] is considered to be a promising candidate for high speed, short range communication systems. In the same context as general line-of-sight communication, the system suffers from shadowing effects. The adoption of a large array antenna offers important features, including multipath-free from the transmission not obstructed by surroundings [1], [5], as channel conditions like fading, are not expected to be severe. Therefore, a single carrier system will be sufficient for a system. The findings in [2], [3], however, point out a different notable degradation issue, intersymbol interference (ISI). The main cause of ISI in [1] is path delay differences among the elements of an array antenna. Due to the adoption of a large array antenna, this path delay difference is large. As a result, the ISI level value also becomes significant. Here, despite the ISI issue arising with a large array antenna, the utilization of equaliz-

ers and LDPC (low-density parity-check code) mitigates the interference issue and bit error rates lower than 10^{-12} can be achieved. However, the adoption of OFDM may increase the complexity in both the transmitting and receiving circuits and OFDM always suffers from PAPR (peak-to-average ratio) problem in transmitter amplifiers.

Estimating the ISI level is of vital importance in evaluating overall system performance. For this, the use of commercial electromagnetic simulation software is limited by memory storage issues due to the large size of the simulation model (in this case the antenna size). In addition, the direct measurement of ISI and related quantities is difficult because of many physical limitations, including cable length, measurement space, and others.

This paper proposes an ISI estimation method based on the near-field distribution of the array antenna as an alternative method to evaluate the ISI for different transmission distances. The method is more convenient than direct measurements as will be indicated in the following sections and also has certain advantages over electromagnetic software simulations as the obtained results closely represent the actual array excitation because the near-field distribution demonstrates defects arising from antenna fabrication. These defects are, however, not easy to measure or predict, so reflecting these imperfections in the antenna modelling for simulation purpose is not practical.

The proposed method can be further applied to predict the communication zone during system planning. Having predicted the ISI, SINR can be obtained as demonstrated in Sect. 5.2. Given the information of the SINR distribution, we can preliminarily predict a communication zone and a shadow zone, as well as the dominant sources of degradation in each zone. This may assist in the system planning to know "how much power should be input to the antenna" and whether "a special modulation technique or a filter should be used to suppress the ISI," and other factors leading to deterioration of the signal.

Overall in this paper, Sect. 2 presents details of the non-far region communication system that is proposed. Here, an evaluation model is derived based on the scenario of the system and will be referred to during the rest of the paper. In Sect. 3, a definition of ISI and the equivalent baseband communication system, from which the ISI formula is derived, are given. The channel transfer function, which is

vital to the ISI analysis, is indicated and will be investigated in detail in the following sections. Section 4 elaborates the ISI estimation method using the near-field distribution: each subsection presents steps in estimating the ISI. Section 5.1 interprets and validates the results obtained by the proposed method. A comparison to direct measurements is provided and discrepancies between the ISI estimated by our proposed method and estimated from direct measurements are discussed. At the end of the section, an application of the ISI in evaluating the signal to noise plus interference ratio (SINR) is given in Sect. 5.2. Finally, we conclude with a discussion of the significance of the proposed method in Sect. 6.

2. Non-Far Region Communication System

In the study here, we focus on the communication scenario shown in Fig. 1. The transmitting (Tx) antenna is a large array antenna and the receiving (Rx) antenna is in a mobile terminal. The important feature of adopting a large array antenna is that it generates an approximately uniform volume over the cross section of the antenna in the non-far region. The rectangular volume forms the reception zone of this system. The distance from the Tx antenna is shorter than $2D^2/\lambda$, where D is the maximum dimension of the transmitting antenna and λ is the wavelength. A user within the reception zone experiences multi-gigabit data access. Figure 2 shows the evaluation model of the system in Fig. 1, in which the Tx antenna is placed at the origin of the rectangular coordinate system. The Rx antenna is represented by a waveguide probe. The coordinate system mentioned hereafter refers to the configuration in Fig. 2.

The actual system is proposed for a 60 GHz-band wireless system at 57–66 GHz. Unfortunately, however, the fabrication of the Tx antenna for the 60 GHz band has not been successfully achieved at present. A 30 GHz-band 64x32-slot array antenna [4] is used for the Tx antenna with corporate feed structure as the feeding circuit. The band discussed in this paper is about a half of the 60 GHz band. The antenna dimensions are $583.2 \times 301.6 \, \mathrm{mm}^2$, directivity 42 dBi, and the aperture efficiency 75%. A WR-28 waveguide probe is used for the Rx antenna.

It should be noted that the frequency scaling (from 60-GHz to 30-GHz) poses no issue of concern for the proposed method. This paper discusses the ISI in the RF band. From the theoretical point of view, the ISI analysis model and method, though frequency-dependent, are the same for all frequencies when the electrical size of the antenna is normalized by the wavelength.

3. Intersymbol Interference Analysis

The following is a discussion of the definition of the ISI and the method to evaluate it quantitatively. First, the section considers a simplified model of a general digital communication system, a so-called equivalent baseband communication system, as the ISI formula will be derived based the
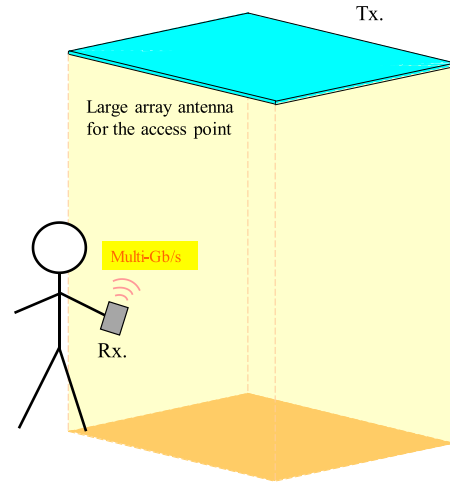

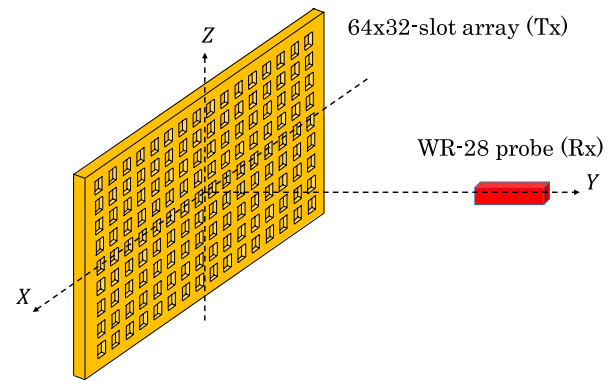**Fig. 1** Non-far region communication system.

Fig. 2 Evaluation model.

given model. Figure 3 shows a model of the equivalent baseband system, which is composed mainly of three parts:1) the transmitted signal (symbol sequence and transmitted filter), 2) the wireless channel, and 3) the received signal (received filter and received digital sequence). From the model, the following can be obtained [2], [3],

$$Y_k = y(kT - nT + \tau_0)$$
$$= \sum_n A_n \int H(f + f_c)G_r(f)G_t(f)e^{j2\pi f[(k-n)T+\tau_0]}df$$
$$= \sum_{n=-\infty}^{\infty} A_{k-n}\Gamma_n, \tag{1}$$

and $\Gamma_m = \int H(f + f_c)G_r(f)G_t(f)e^{j2\pi f[mT+\tau_0]}df$, (2)

where f_c is the center frequency, T is the symbol period, and τ_0 is the time of flight between the Tx antenna element closest to the Rx antenna to the Rx antenna, which by definition is the value that maximizes the desired signal level. The transmitted digital sequence $\{A_n\}$ is a discreet complex stochastic variable and has an i.i.d. property which satisfies the following equations,
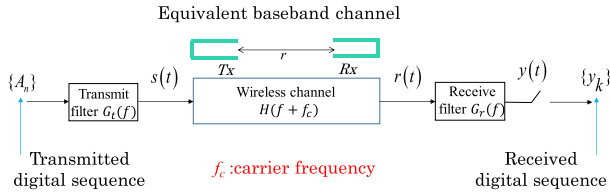
$$E[A_n] = E[A_n*] = 0,$$

Fig. 3 Equivalent baseband communication system.

$$E[A_n A_m] = E[A_n A_{m*}] = 0 \text{ for } m \neq n,$$
$$E\left[|A_n|^2\right] = A' \text{ for a real constant } A'.$$

The term $A_k \Gamma_0$ is referred to as a desired signal component and the other the terms together form the interference. The ISI is defined as the ratio of the power of the interference over the desired signal power and it is expressed as follows,

$$
ISI = \frac{E\left[\left|\sum_n A_n \Gamma_{k-n}\right|^2\right] - \max_n E\left[|A_n \Gamma_{k-n}|^2\right]}{\max_n E\left[|A_n \Gamma_{k-n}|^2\right]}
$$
$$
= \frac{\sum_n |\Gamma_{k-n}|^2 - \max_n |\Gamma_{k-n}|^2}{\max_n |\Gamma_{k-n}|^2} \tag{3}
$$

Given that the symbol sequence is independently and identically distributed with a zero mean value, [2], [3] provide further details; ISI is therefore determined by the channel coefficient Γ_m. Considering the expression of Γ_m in Eq. (2), in general, the product of $G_r(f)G_t(f)$ constitutes a raised-cosine filter [9], the parameters of which are specified for a specific communication system. The unknown parameters here are the channel transfer function $H(f + f_c)$, which is characterized by the wireless channel, and the time of flight τ_0. Having determined the channel transfer function $H(f + f_c)$, ISI given in Eq. (3) may be computed via the numerical integration of Eq. (2)

In this study, the ISI is mainly determined by the electrical size of the Tx antenna and the symbol rate. The definition of ISI in Eq. (3) is derived based on the equivalent baseband communication system shown in Fig. 3, where no assumptions of the number of antennas, transmission distance, or symbol rate are specified. This makes Eq. (3) applicable for any number of antennas, transmission distances, and symbol rates. Though the number of Tx and Rx antennas is not specified in the equivalent baseband communication system, the definition of the channel transfer function $H(f + f_c)$ needs to be modified in the case of multiple Tx and Rx antennas. This paper discusses only the situation of a single Tx and Rx antenna. Cases with multiple Tx and Rx antennas will be discussed in a future study.

4. ISI Estimation Using Near-Field Distribution

In the previous section, the important parameters and expressions required to compute ISI are presented and as mentioned there, the unknown parameter is the channel transfer function. Depending on the wireless channel components (the Tx antenna, the Rx antenna, and the propagation environment), the estimation of its characteristic function might be very complicated even with the help of simulation software. To get around this problem, we limit our consideration to the situation shown in Fig. 2. Also, the evaluation model is appropriate for our system because this system preference is line of sight and multipath effects from the surroundings, [1], [5], which are suppressed due to the adoption of a large array antenna (such as the 64x32-slotted array antenna here) to make a uniform field in a rectangular volume in the non-far region. Unfortunately, even for the case of this model, the antenna size however prevents using electromagnetic simulation software.

In this section, we introduce the method to evaluate the channel transfer function and ISI in detail using the near-field distribution of the array antenna in consideration here.

4.1 Measurement of the Near-Field Distribution

The first step in evaluating the channel transfer function is the near-field measurement of an antenna in consideration. In this study, the near-field measurement is conducted on a 64x32-slot array antenna. The measurement details are as follows,

1) Measured area: $600 \times 320 \text{ mm}^2$
2) Sampling interval: 4 mm
3) Frequency range: 29.06–30.14 GHz
4) Number of the measured frequencies: 37

The measurement area has to be sufficiently much larger than the size of the array antenna being tested. However, the larger the measurement area, the longer the measurement time, as the sampling interval has to be smaller than one half of the wavelength of the lowest measured frequency. The frequency range is scaled down to half of the transmission bandwidth (2.16 GHz) of the channel in the 60 GHz-band system. As for the number of the measured frequencies, it is preferable to measure as many frequency points as possible to obtain accurate details of the frequency characteristics across the whole band (29.6–30.14 GHz). More measured frequencies result in a longer measurement stage however, and a trade-off has to be considered. Figures 4(a)–(f) show the amplitude and the phase of the near-field distributions at the edge and center of the band, showing that the amplitude and phase varied within 3 dB and 60 degrees over almost all of the array aperture. The non-uniformity in the field distribution of the array antenna is clearly reflected through these results of the near field measurements. And results are difficult to predict using simulation software as we have no way of knowing how much and where errors occur in the antenna after fabrication.

4.2 Estimation of Channel Transfer Function

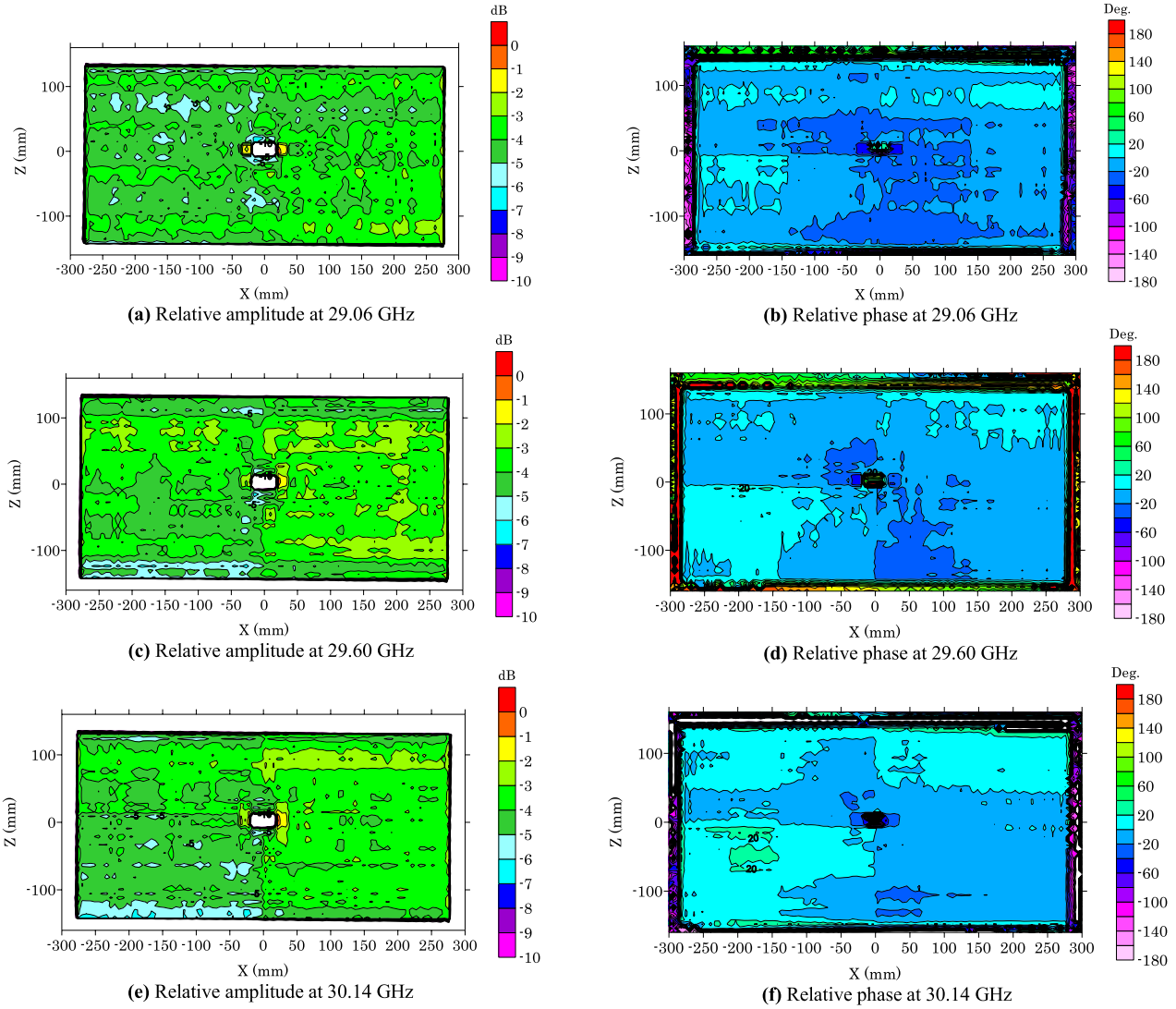With the near-field distributions for various frequencies in

(a) Relative amplitude at 29.06 GHz

(b) Relative phase at 29.06 GHz

(c) Relative amplitude at 29.60 GHz

(d) Relative phase at 29.60 GHz

(e) Relative amplitude at 30.14 GHz

(f) Relative phase at 30.14 GHz

Fig. 4 Near-field distribution.

Sect. 4.1, the fields at the Rx antenna can be estimated. This can be achieved by mean of dipole approximation as illustrated in Fig. 5. The amplitude and the phase values of each sampling represent those of magnetic current dipoles at the corresponding position. As a result, the slot array antenna can be replaced by the array of infinitesimal magnetic-current dipoles, the amplitude and the phase of which are determined by those of the near-field distribution. By summing the total contribution from each dipole, the fields at the Rx antenna radiated from the Tx antenna are obtained for each measured frequency. Assuming that the receiving frequency characteristics of the Rx antenna are approximately uniform (which is true for the case of a waveguide probe WR-28), the channel transfer function $H(f + f_c)$ can be represented by the field radiated by the Tx antenna, see Eq. (A· 6). This makes it possible to obtain a discreet channel transfer function (37 points) using the near-field distribution.

To extend this procedure to a continuous function, interpolation is required, and here spline interpolation is
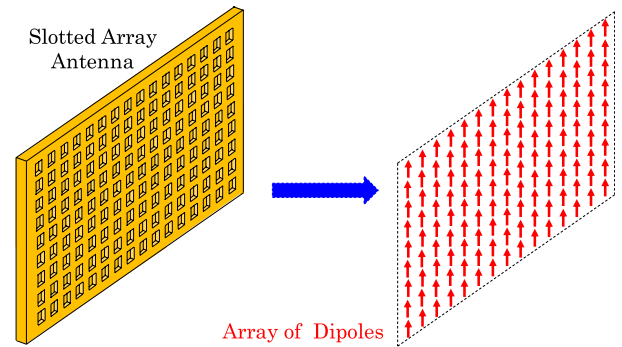

Fig. 5 Dipole approximation on array antennas.

applied to create a smoothly continuous function [8]. A discreet channel transfer function composed of the 37 frequency points is determined from the fields at the corresponding measured frequencies. Then, with a continuous channel transfer function interpolated from the discreet chan-
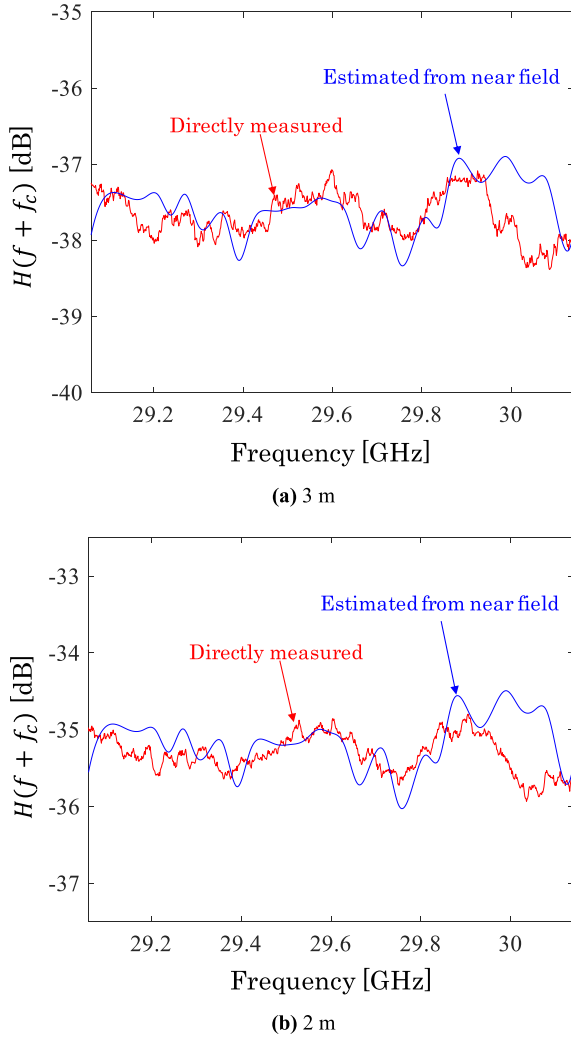
(a) 3 m

(b) 2 m

Fig. 6 S21 plots.

nel transfer function (37 points) using spline interpolation, Figs. 6(a)–(b) show examples of the channel transfer function ($H(f + f_c)$) estimated from the near-field distribution (blue line). The red line shows the directly measured $H(f + f_c)$. The $H(f + f_c)$ estimated from the near-field distribution shows a similar appearance as that of the direct measurement except in the 30 GHz to 30.14 GHz frequency range. This disagreement is likely caused by the shift of the Rx antenna position from the center of the Tx antenna. In the non-far region, a slight shift can significantly change S_{21} (this effect over ISI will be discussed further in Sect. 5). Also, the rate of change in the fields increases with the frequency increases, probably leading to the disagreements at the high frequency range.

4.3 ISI Calculation

The above suggests a way to determine the channel transfer function is available. The ISI can be computed using Eqs. (2) and (3). First, the channel coefficient Γ_0 is computed using the integral expression in Eq. (2) performed using numerical

integration (Simpson's rule). Concurrently, the time of flight τ_0 has to be searched for, numerically, to maximize Γ_0. In the case of ideally uniform excitation, τ_0 is equal to $t_{\min}$: the propagation time from the center of the array to the observation point on the Z axis according to Fig. 2. For the general case, τ_0 is determined from the interval $[t_{\min} - 5T, t_{\min} + 5T]$ where T is the symbol period. This interval is specified based on the time of flight having to be around $t_{\min}$ as our desired symbol first arrives at the receiver at $t_{\min}$, the slowest desired symbol should arrive within T seconds after the first. Taking into account the characteristics of an inverse raised cosine function, the peak value would lie within $[t_{\min} - 2T, t_{\min} + 2T]$ after total interference. Here, $5T$ is used to ensure that error due to the approximate prediction of the position of the peak value is compensated for. After τ_0 is determined, all the channel coefficients Γ_n (including Γ_0) can be computed using τ_0. The parameters required to calculate Eq. (2) are given as follows,

1) Center frequency: $f_c = 29.6$ GHz
2) Symbol period: $T = 1.17$ ns
3) Bandwidth: $BW = 1.08$ GHz
4) Roll-off filter: $\beta = 0.25$ (see Appendix).

At this point all the channel coefficients Γ_n are known, and ISI can be computed via Eq. (2). Though the limit of summation in Eq. (2) is infinite, the computation of such terms is possible through truncation. In fact, here the truncation is justified because of the characteristics of the inverse raised-cosine that is a one-side decreasing function. This ensures that Γ_n decreases as $|n|$ increases. The results given in the following section were estimated assuming that A_k (Γ_0) is the desired signal and interference terms are truncated to 10 terms:

$$\begin{cases} A_{k-5}(\Gamma_5), A_{k-4}(\Gamma_4), A_{k-3}(\Gamma_3), A_{k-2}(\Gamma_2), A_{k-1}(\Gamma_1), \\ A_{k+1}(\Gamma_{-1}), A_{k+2}(\Gamma_{-2}), A_{k+3}(\Gamma_{-3}), A_{k+4}(\Gamma_{-4}), A_{k+5}(\Gamma_{-5}) \end{cases}$$

5. Results

This section presents a discussion of results of the discussion developing the method proposed here as well as experiment based results are included. Direct measurements of ISI are difficult and the determine ISI experimentally, we measured a related quantity, $H(f + f_c)$. The quantity ($H(f + f_c)$), is directly related to ISI and determine a value for severity of ISI for a communication system. In this way, an experiment based ISI can be obtained from the directly measured $H(f + f_c)$ by following the method detailed in the previous section.

Before conidering the results of the disscussion of the proposed method and the experimentally determined ISI, it is useful to recall the physical interpretation of ISI for a large array antenna. The situation giving rise to an ISI is that signals follow different paths resulting in differences in delays, and as the result signals arrive at the receiver at different times and symbols then interfere with each other. In the case here with a large array antenna, signals travel from different elements to a receiver and undergo different
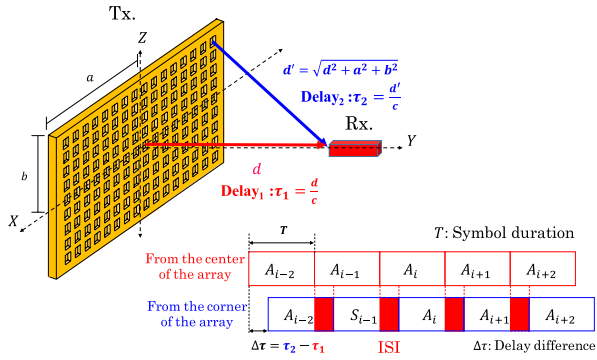
Fig. 7   Graphical Visualization of the ISI arising in a large array antenna.

Fig. 8   Plots of ISI values under different excitations.

path delay (the adoption of a corporate feed circuit in the Tx antenna makes the internal delay negligible) due to the large size of the array, the effect on signals traveling from the center of the array and the corner of the array is different, as suggested in Fig. 7. The delay difference is large when the receiver is close to the array and a large value of ISI can be expected. In this case, the differences in the delay decrease for the receiver fauther away from the array and result in smaller ISI value, put generally, ISI decreases as the transmission distance increases.

5.1   ISI Comparison with Direct Measurement

Figure 8 illustrates the ISI results for various cases. The red line represents the ISI estimated from the near-field distribution and the blue curve indicates the ISI for the ideally uniform excitation (both the amplitude and the phase of the near-field distribution are uniform). The ISI for the ideally uniform excitation is smaller than that of the actual excitation in the antenna because of the uniformity in field excitation for distances longer than 50 cm. The black starlike dots show the ISI values obtained by the directly measured $H(f + f_c)$. Comparing these values, the ISI results estimated by the proposed method and the directly measured ones are similar but not in complete agreement. The discrepancy may be attributed to shifts in the Tx and Rx antennas as will be demonstrated below. One of difficulties in the direct $H(f + f_c)$ measurement is the alignment between the Tx and the Rx antennas. Even with a 3D scanner, it is still not straightforward to align the Tx and the Rx antennas. As the Rx antenna is in the non-far region where fields change very much, a small shift would cause a change in the $H(f + f_c)$ prediction as well as in the ISI. In consideration of this, the effect of a shift can be quantified, and the blue curves in Fig. 9 show the upper and lower boundaries of possible ISI values evaluated by assuming that the Rx antenna is shifted within ±3 cm horizontally and ±1 cm vertically. The region within these boundaries show the possible ISI values when the shift is included. It is clear that all the ISI results estimated from directly measured $H(f + f_c)$ lie within this region, strongly suggesting that the shift of the Rx antenna from the Tx antenna can account for the discrepancies between the ISI results. Note that the shift range of 3 cm is
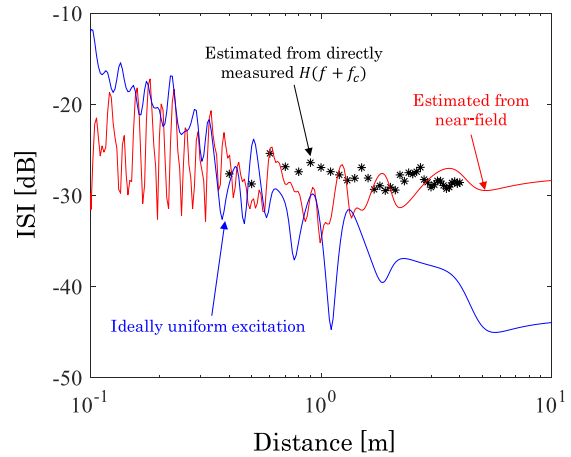
acceptable in practice as, at a distance of 2 m, a 1-degree horizontal (or vertical) deviation by the probe corresponds to a 3.5 cm shift horizontally (or vertically) in the probe position.

The reasons why this study is able to conclude that the shift in the position of the Rx antenna is dominant in our proposed ISI analysis method are:

1) The Rx antenna is in the near field region where a slight change in position may result in a significant change in the receiving field. The effect detailed above also reflects the results in Figs. 8–10 where the ISI discrepancy, both between the ISI results estimated from the measured results and near-field at the center of the Tx antenna, and also between the ISI results estimated from the measured results and near-field including the shift, decrease as the transmission distance increases because the receiving field at the Rx antenna increasingly behaves as a field in the far-field region with increasing distance between the Tx and the Rx antennas; also substantiating that a shift in the Rx antenna position in the Tx antenna plane has an insignificant effect on the ISI level (value) far from the Tx antenna. When the transmission distance is shorter, the shift in the Rx position would cause a larger change in the ISI level, as in Figs. 9, 10. For the experiments, a 3D scanner was not avialable and the alignment between the Tx and the Rx antennas was performed manually, making the alignment between the Tx and Rx antennas susceptible to error.

2) The coverage of the compact -range communication system is in the non-far region and within the cross-sectional area of a Tx antenna (a large array antenna). For such a situation, it is suitable that the ISI value is estimated within an area (or more specifically a rectangular volume) rather than based on a point-wise estimation and that the possible values of the ISI are indicated in that particular area. Conclusively, the estimation of ISI including the effect of any shift is practical and acceptable.

Still, it should be borne in mind that this study simplifies the analysis (Sect. 3) of the ISI value by assuming that the Rx antenna receives the field radiated by the Tx antenna with-
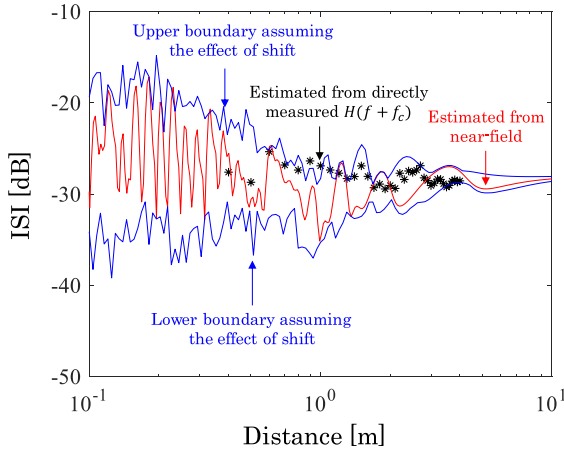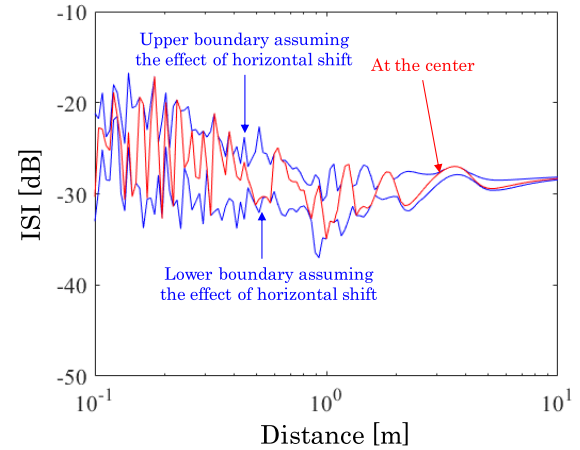
Fig. 9 ISI variation due to shifts in the Rx antenna.

(a) Horizontal shift

(b) Vertical shift

Fig. 10 Influence of antenna shifts on the ISI.

out disturbance of the Tx antenna or the system itself. This implies that theoretically multiple reflection effects between the Tx and the Rx antennas are disregarded. For a valid-itation of the method proposed here, a measurement result free of multiple reflections is desirable. However, in actual measurements this effect cannot be avoided. The multiple reflection effect increases as the transmission distance short-ens, especially in the near-field region as is clearly shown in the case of this study. In turn, this may unavoidably have af-fected the measurement results and it is difficult to calculate how large an effect this has had on the experiments here. In future study, we will include modifications of the analysis by taking the multiple reflection effects into account bearing in mind that this will increase the complexity of the method of the analysis.
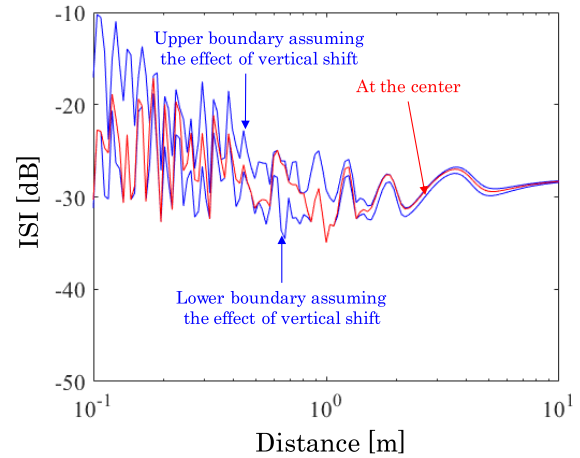
To discriminate the influence of the horizontal and ver-tical shifts, the ISI boundaries were calculated separately for the horizontal and vertical shifts within ±2 cm as shown in Figs. 10(a) and 10(b). Here the shift along the horizontal axis affects ISI especially at distances far from the antenna more than it affects that along the vertical axis. The physical reason for this difference in the behaviour can be explained by the near-field distribution. The ISI variation by the horizontal shift is affected by differences in the near-field distribution between the left and right sides of the array aperture, while that by the vertical shift is affected by the differences between the upper- and lower-half sides. Looking at the near-field dis-tributions in Fig. 4, we can see that the difference between the left and the right sides is larger than that between the upper-half and the lower-half sides. This difference is cer-tain to affect $H(f + f_c)$. It may be concluded that ISI is affected more strongly by the shift along the horizontal axis than that along the vertical axis at distances far from the Tx antenna.

5.2 Application to the Signal to Noise plus Interference Ratio (SINR)

In this subsection, the signal to noise plus ratio (SINR) is estimated using the estimated ISI from the previous subsec-

tion and, at the end of the present subsection, the effect of ISI and noise on the communication quality is discussed. For this, first, the received power has to be determined. The received power can be expressed as a function of $H(f + f_c)$ and the input power P_{in}, as in Eq. (A· 1) in the Appendix. Assuming the input power to the array $P_{in} = 1$ (mW). The re-ceived power at various distances can be readily determined as shown in Fig. 11.

Noise is one degradation factor which is caused by the electronics devices and by the ambience. Thermal noise is commonly considered, and assuming a noise figure value of the system as 10 dB [6], the noise temperature is 300 K and the receiver bandwidth equal to 1.08 GHz. Then the thermal noise power is given by
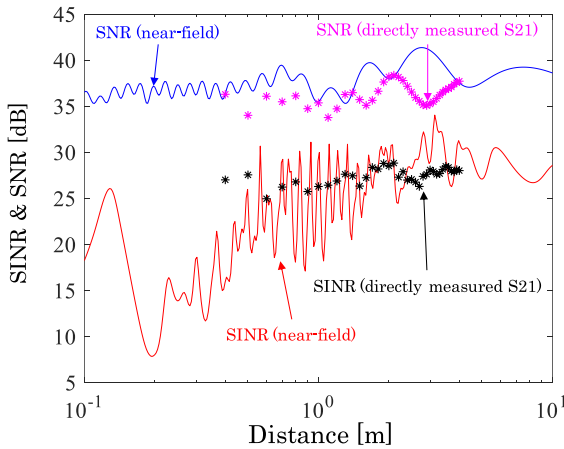
$$N.F. \times kBT = 10 \times (1.38 \times 10^{-23})(1.08 \times 10^9)(300)$$
$$= -73.5 \, \text{dBm}$$

As detailed further in Eq. (A· 2) in the appendix. This makes it possible for SNR to be evaluated, and the distribution of interference from each element to the receiver becomes $I_i; i = 1, 2, \ldots, 64 \times 32$ with the total interference at the
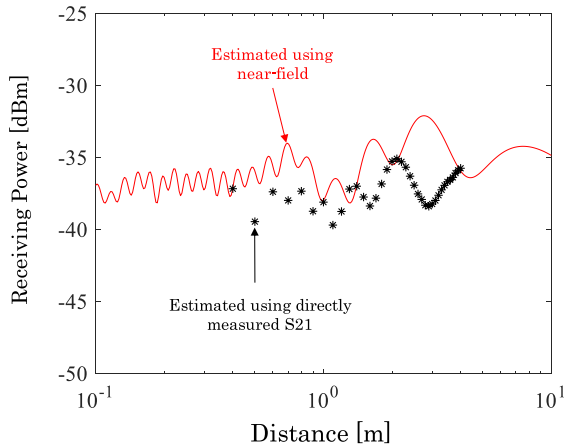
Fig. 11 Receiving power comparison.

Fig. 12 SINR & SNR comparison.

receiver $I_{re} = I_1 + I_2 + \ldots + I_{64\times32}$. From the central limit theorem [6], the distribution of I_{re} can be approximated by a Gaussian distribution, as the number of elements, 64×32, is large. Finally, SINR can be calculated using Eq. (A·3) in the appendix and the results of SINR and SNR are shown in Fig. 12. It can be seen that SINR is larger than SNR. Given the fact that the intended transmission distance for the system is normally up to 10 m it may be concluded that ISI is the dominant factor for the system.

6. Conclusion

A method for estimating ISI from the near-field distribution is proposed as a promising alternative to predict ISI in a non-far region system using large array antennas. The ISI estimation by means of the proposed method is demonstrated. The influence of uniformity in antenna excitation on ISI is indicated. The ISI estimated from the near-field distribution is compared with the ISI estimated from directly measured $H(f + f_c)$ values. The results are in good agreement, though some discrepancies are observed. The shifting of the Rx antenna from the Tx antenna is shown to account for the discrepancy. The ISI boundary is estimated by tak-

ing the shift into account. Finally, SINR, as well as SNR, are estimated from the ISI results obtained for both, and the ISI is shown to be the dominating factor over noise for the current situation. This implication strongly suggests that ISI estimation is important in designing communication systems like that considered here.

References

[1] M. Zhang, K. Toyosaki, J. Hirokawa, M. Ando, T. Taniguchi, and M. Noda, "A 60 GHz-band compact-range gigabit wireless access system using large array antennas," IEEE Trans. Antennas Propag., vol.63, no.8, pp.3423–3440, Aug. 2015.
[2] M. Zhang, M. Wakasa, K. Araki, J. Hirokawa, and M. Ando, "Analysis of intersymbol interference in a 60 GHz-band compact-range wireless access system using various large array antennas," Intl. Symp. Antennas Propag., S3.3.4, Nov. 2015.
[3] M. Wakasa, M. Zhang, J. Hirokawa, K. Araki, and M. Ando, "Intersymbol interference analysis of a compact-range high-speed wireless communication system using travelling-wave-fed slot arrays," IEICE Technical Report, AP2015-45, July 2015.
[4] D. Kim, J. Hirokawa, M. Ando, J. Takeuchi, and A. Hirata, "64x64-element and 32x32-element slot array antennas using double-layer hollow-waveguide corporate-feed in the 120 GHz band," IEEE Trans. Antennas Propag., vol.62, no.3, pp.1507–1512, March 2014.
[5] M. Ali and M. Ando, "Fast estimation of shadowing effects in millimeter-wave short range communication by modified edge representation," IEICE Trans. Commun., vol.E98-B, no.9, pp.1873–1881, Sept. 2015.
[6] C.A. Balanis, Advanced Engineering Electromagnetics, pp.133–151, John Wiley & Sons, New York, 1989.
[7] A.L. Garcia, Probability, Statistic, and Random Processes for Electrical Engineering, pp.359–375, Pearson Prentice Hall, New Jersey, 2008.
[8] M. Hazewinkel, ed., Encyclopaedia of Mathematics, vol.3, pp.270–272, Kluwer, 1994.
[9] S.S. Haykin, Communication Systems, pp.247–267, John Wiley & Sons, New York, 2001.
[10] K.F. Riley, M.P. Hobson, and S.J. Bence, Mathematical Methods for Physics and Engineering, pp.415–427, Cambridge Univ. Press, Cambridge, 2006.
[11] T. Zhang, L. Li, M. Xie, H. Xia, X. Ma, and T.J. Cui, "Low-cost aperture-coupled 60-GHz-phased array antenna package with compact matching network," IEEE Trans. Antennas Propag., vol.65, no.12, pp.6355–6362, 2017.

Appendix:

Receiving power

Let the modulated signal to be transmitted be defined as follows,

$$s(t) = \sum_n A_n g(t - nT)e^{j2\pi f_c t},$$

$$s(t) = \left(\sum_{n=-\infty}^{\infty} A_n \delta(t - nT)\right) * g_t(t),$$

$$= \int_{-\infty}^{\infty} \sum_{n=-\infty}^{\infty} A_n \delta(\tau - nT)g_t(t - \tau)d\tau$$

where $\{A_n\}$ is a random sequence defined in Sect. 3 and $g(t)$

is the time domain of the pulse shaping filter $G(f)$. Then, the input power is given by

$$P_{in} = A' f_T \int |G(f)|^2 \, df.$$

The integration is carried over the bandwidth of interest.

The received signal can be expressed as

$$y(t) = \sum_n A_n \left(g(t - nT)e^{j2\pi f_c t} \right) * h(t),$$

where $*$ is the convolution integral operator and $h(t)$ is the impulse response of a wireless channel. As a result, the receiving power is defined as follows,

$$P_{re} = A' f_T \int |G(f)H(f + f_c)|^2 \, df$$

or

$$P_{re} = \frac{P_{in}}{\int |G(f)|^2 \, df} \int |G(f)H(f + f_c)|^2 \, df, \tag{A·1}$$

given that $H(f)$ is the Fourier transform of $h(t)$.

Signal to Noise plus Interference Ratio (SINR)

The variance in thermal noise is as follows,

$$N = kBT \tag{A·2}$$

given that k is the Boltzmann constant, B is the receiving bandwidth of a receiver, and T is the noise temperature, then SINR is simply defined as follows,

$$SINR = \frac{P_{re}}{N + ISI \times P_{re}} \tag{A·3}$$

ISI Formula

Referring to the equivalent baseband communication system in Fig. 3, we have

$$s(t) = \left(\sum_{n=-\infty}^{\infty} A_n \delta(t - nT) \right) * g_t(t)$$

$$= \int_{-\infty}^{\infty} \sum_{n=-\infty}^{\infty} A_n \delta(\tau - nT) g_t(t - \tau) d\tau = \sum_{n=-\infty}^{\infty} A_n g_t(t - nT),$$

where $*$ represents a convolution operator. $g_t(t)$ and is the inverse Fourier transform of the transmitting filter $G_t(f)$. Then, the signal $s(t)$ is transmitted through the wireless channel $h(t)$, with the Fourier transform of $H(f + f_c)$, resulting in the received signal $r(t)$ expressed as follows,

$$r(t) = \sum_{n=-\infty}^{\infty} A_n x(t - nT).$$

Here, $x(t) = g_t(t) * h(t)$. In the same manner, the output signal $y(t)$ to the Rx filter is given by,

$$y(t) = \sum_{n=-\infty}^{\infty} A_n \Gamma(t - nT),$$

where $\Gamma(t) = x(t) * g_r(t)$ and $g_r(t)$ is also the inverse Fourier transform of $G_r(f)$. We can express $\Gamma(t)$ in terms of a spectral function as follows,

$$\Gamma(t) = \int_{-\infty}^{\infty} G_t(f)H(f + f_c)G_r(f)e^{j2\pi ft} df.$$

Subsequently, the received signal $y(t)$ is sampled at the rate of $kT + \tau_0$ for $k = 0, 1, 2, \ldots$ the τ_0 represents the transmission delay through the channel, referred to as the time of flight. The output to the sampling process is the discreet information-bearing sequence $\{y_k\}$ which is expressed below,

$$y_k = \sum_{n=-\infty}^{\infty} A_n \Gamma(kT - nT + \tau_0)$$

$$= \sum_{n=-\infty}^{\infty} A_n \Gamma_{k-n} \tag{A·4}$$

$$= \sum_{n=-\infty}^{\infty} A_n \int_{-\infty}^{\infty} G_t(f)H(f + f_c)G_r(f)e^{j2\pi f(kT - nT + \tau_0)} df.$$

We can distinguish a sampled sequence into two parts:

$$y_k = A_k \Gamma_0 + \sum_{n \neq k} A_n \Gamma_{k-n}. \tag{A·5}$$

The first term on LHS of Eq. (A·5) is the desired information symbol. The other terms here express interference. The ISI is defined as the ratio of the interference power over the desired symbol power:

$$ISI = \frac{E\left[\left| \sum_n A_n \Gamma_{k-n} \right|^2 \right] - \max_n E\left[|A_n \Gamma_{k-n}|^2 \right]}{\max_n E\left[|A_n \Gamma_{k-n}|^2 \right]}$$

$$= \frac{\sum_n |\Gamma_{k-n}|^2 - \max_n |\Gamma_{k-n}|^2}{\max_n |\Gamma_{k-n}|^2}.$$

Relation between Fields and Channel Transfer Function

First, we assume that the transmitted signal is represented by the variation in electric (or magnetic) current density. With a model of an antenna represented by a current source $j(t)$, where, for simplicity, we assume that $j(t)$ is aligned in the z direction and lets $J(f)$ be the spectral of $j(t)$ shown as follows,

$$j(t) = \int_{-\infty}^{\infty} J(f)e^{j2\pi ft} df$$

$$= \lim_{\Delta f \to 0} \sum_{n=-\infty}^{\infty} J(f_n) e^{j2\pi f_n t} \Delta f.$$

Let $\vec{E}(f)$ be a solution to the time harmonic Maxwell's equation. By the superposition principle, the field $\vec{\xi}(t)$ produced by the source $j(t)$ can be expressed by

$$\vec{\xi}(t) = \lim_{\Delta f \to 0} \sum_{n=-\infty}^{\infty} J(f_n) \vec{E}(f_n) e^{j2\pi f_n t} \Delta f.$$
$$= \int_{-\infty}^{\infty} J(f) \vec{E}(f) e^{j2\pi f t} df.$$

For the receiver, we suppose that it is linearly polarized in the z direction and its receiving characteristic in the frequency domain is defined as $\Lambda(f)$ (In practice, a waveguide probe is linearly polarized in a certain direction). Therefore, the receiving signal $r(t)$ is expressed as follows,

$$r(t) = \int_{-\infty}^{\infty} \Lambda(f) J(f) E_z(f) e^{j2\pi f t} df.$$

As a result, we conclude that the channel transfer function is related to the E-field via

$$H(f) = \Lambda(f) J(f) E_z(f), \qquad (A \cdot 6)$$

where E_z is the z component of the E-field.

Kiyomichi Araki was born in 1949. Received the Ph.D. degree in physical electronics from Tokyo Institute of Technology, Tokyo, Japan, in 1978. In 1973–1975, and 1978–1985, a Research Associate at Tokyo Institute of Technology, and in 1985–1995 an Associate Professor at Saitama University, Saitama, Japan. In 1979–1980 and 1993–1994, a Visiting Research Scholar with the University of Texas, Austin, TX, USA, and University of Illinois, Urbana, IL, USA. From 1995 to 2014, he was a Professor at Tokyo Institute of Technology. He has numerous journals and peer reviewed publications in RF ferrite devices, RF circuit theory, electromagnetic field analysis, software-defined radio, array signal processing, UWB technologies, wireless channel modeling, MIMO communication theory, digital RF circuit design, information security, and coding theory. Dr. Araki was awarded the Best Paper Award in 2007 and a Fellow of IEICE from 2004. He is a president-elect of the Electronics Society of IEICE of Japan and a member of IEE and the Information Processing Society of Japan. He served as a Steering Committee Chair of APMC2010, and is the Chair of the MTT-S Japan chapter. He was the Director, Finance of IEICE in 2013.

Jiro Hirokawa received the B.S., M.S. and D.E. degrees in electrical and electronic engineering from Tokyo Institute of Technology (Tokyo Tech), Tokyo, Japan in 1988, 1990 and 1994, respectively. A Research Associate from 1990 to 1996 and an Associate Professor from 1996 to 2015 at Tokyo Tech. He is currently a Professor there. He was with the antenna group of Chalmers University of Technology, Gothenburg, Sweden, as a Postdoctoral Fellow from 1994 to 1995. His research area has been in slotted waveguide array antennas and millimeter-wave antennas. He received the IEEE AP-S Tokyo Chapter Young Engineer Award in 1991, the Young Engineer Award from IEICE in 1996, the Tokyo Tech Award for Challenging Research in 2003, the Young Scientists' Prize from the Minister of Education, Cultures, Sport, Science and Technology in Japan in 2005, Best Paper Award in 2007 and a Best Letter Award in 2009 from IEICE Communications Society, and a IEICE Best Paper Award in 2016. He is a Fellow of IEEE.

Tuchjuta Ruckkwaen received the B.S. and M.S. degrees in Electrical Engineering from Chulalongkorn University and Tokyo Institute of Technology in 2015 and 2018, respectively. Currently, he is working toward the D.E. degree at Tokyo Institute of Technology (Tokyo Tech), Tokyo, Japan with research interests in high-frequency diffraction and high-gain millimeter-wave antennas.

Takashi Tomura was born in Sendai, Japan. Received the B.S., M.S. and D.E. degrees in electrical and electronic engineering from the Tokyo Institute of Technology, Tokyo, Japan, in 2008, 2011 and 2014, respectively. A Research Fellow of the Japan Society for the Promotion of Science (JSPS) in 2013. From 2014 to 2017, at Mitsubishi Electric Corporation, Tokyo engaged in research and development of aperture antennas for satellite communications and radar systems. Currently a Specially Appointed Assistant Professor at the Tokyo Institute of Technology, Tokyo with research interests in electromagnetic analysis, aperture antennas and planar waveguide slot array antennas.

Makoto Ando   was born in Hokkaido, Japan, on February 16, 1952. He received the B.S., M.S. and D.E. degrees in electrical engineering from Tokyo Institute of Technology, Tokyo, Japan in 1974, 1976 and 1979, respectively. From 1979 to 1983, worked at Yokosuka Electric Communication Laboratory, NTT, and was engaged in development of antennas for satellite communication. A Research Associate at Tokyo Institute of Technology from 1983 to 1985, and is currently a Professor. His main interests have been high frequency diffraction theory such as Physical Optics and Geometrical Theory of Diffraction. His research also covers the design of reflector antennas and waveguide planar arrays for DBS and VSAT. Latest interest includes the design of high gain millimeter-wave antennas. Dr. Ando received the Young Engineers Award of IEICE Japan in 1981, the Achievement Award and the Paper Award from IEICE Japan in 1993. He also received the 5th Telecom Systems Award in 1990, the 8th Inoue Prize for Science in 1992, the Meritorious Award of the Minister of Internal Affairs and Communications and the Chairman of the Broad of ARIB in 2004 and the Award in Information Promotion Month 2006, the Minister of Internal Affairs and Communications. He served as the guest editor-in-chief of more than six special issues in IEICE, Radio Science and IEEE AP. He serves as the Chair of Commission B of URSI 2002–2005 and the member of Administrative Committee of IEEE Antennas and Propagation Society 2004–2006. He was the chairs of the Technical committee of Electromagnetic theory (2004–2005) and Antennas and Propagation (2005–2007) in IEICE. He was the general chair of the 2004 URSI EMT symposium in Pisa and of the ISAP 2007 in Niigata. He was the 2007 President of Electronics Society IEICE and also the 2009 President of IEEE Antennas and Propagation Society. He served as the 2007–2009 Program Officer for engineering science group in Research Center for Science Systems, JSPS.